Acta Mechanica 164, 115–138 (2003)
DOI 10.1007/s00707-003-0022-9

Acta Mechanica
Printed in Austria

Bifurcations of parametric oscillations of beams with three equilibria

K. V. Avramov, Kharkov, Ukraine

Received December 2, 2002; revised May 20, 2003
Published online: September 8, 2003

Summary. Nonlinear curvature and nonlinear inertia are taken into account in the beam model. The constant part of the parametric force is proposed to be greater than the buckling one, therefore the beam has three equilibria. One-mode approximation of the beam oscillations is used. Bifurcations of the beam oscillations are analyzed by Melnikov's method. Moreover, beam oscillations close to the stable equilibriums are studied by the multiple scales method.

1 Introduction

Oscillations of continuous systems with several equilibria are encountered frequently in engineering sciences [1]. The theory of such systems has been advanced significantly due to the Melnikov method [2]–[7]. In these publications one-mode approximations of continuous systems were considered. Using these approximations, one-degree-of-freedom nonlinear oscillators were derived. These oscillators were considered by many authors. Duffing oscillator trajectories close to the resonance energy levels were studied by A. D. Morozov [8]. He derived the system of two autonomous differential equations, which governed these motions. P. Holmes [3] studied beam dynamics by the Melnikov method. The Duffing-van der Pol oscillator was considered in the paper [9], where the repeated bifurcations of the periodic motions close to the resonance energy levels were studied. As follows from [10], the numerical results of the Duffing equation coincide qualitatively with the analytical analysis of the motions close to the resonance energy levels. The mathematical theory of the motions close to the resonance energies levels was considered by A. D. Morozov and L. P. Shil'nikov [11]. This theory was used to analyze invariant tori and their synchronization [12]. The system with the nonlinear parametric term was considered in [13]. Chaotic oscillations of a beam in a magnetic field were analyzed experimentally by F. Moon [14]. As follows from this paper, the beam has three or five equilibria. R. Chason and J. D. Bejarano [15] used Melnikov homoclinic functions to study an oscillator with five equilibria. Oscillations close to the equilibria were considered in [16], [17]. As follows from these papers, such oscillations undergo period-doubling bifurcations. An effect of the different excitations on the dynamics of the Duffing system was studied in [18]. The homoclinic Melnikov function of the Duffing oscillator with the parametric excitation was derived in [19].

The systematic treatment of the parametric oscillations theory was presented in the monograph [20]. H. A. Evensen and R. M. Ivan-Iwanowsky [21] considered column parametric

oscillations taking account of the nonlinear inertia. K. Eisinger and H. C. Merchaut [22] took into account the rotatory inertia and longitudinal motions of beams. H. Saito and N. Koizumi [23] analyzed parametric oscillations of hinged beams. K. Sato, H. Saito and K. Otomi [24] analyzed parametric oscillations of a beam with a concentrated disc. R. F. Fung [25] studied parametric vibrations taking into account the nonlinear inertia.

Dynamics of the beam with three equilibria under the action of a parametric periodic excitation is considered in this paper. Nonlinear inertia and nonlinear curvature are taken into account in the beam model. Using Galerkin's method, the nonlinear partial differential equation is transformed into a second order ordinary differential equation. Using the subharmonic Melnikov function, the saddle-node bifurcations are investigated. The topology of the flow close to the resonance energy levels is considered. Periodic oscillations and bifurcations of the beams close to equilibrium are analyzed.

2 Problem formulation

Figure 1 shows the beam under consideration. Mass M is attached to the end of the beam. Transverse beam motions $W(s,t)$ induce displacements $\eta(t)$ of the mass M. Therefore, the linear viscous damping force $R_L = c_L\dot{\eta}$ acts on mass M. The nonlinear curvature and nonlinear inertia are taken into account in the beam model [20]. The parametric oscillation equation has the form:

$$EJw'''' + \frac{EJ}{2}\left(w''w'^2\right)'' + \left\{P_0 + P_t\cos(\bar{\Omega}t) - \frac{M}{2}\int_0^l (w'^2)''_{tt}\,ds - \frac{c_L}{2}\int_0^l (w'^2)'_t\,ds\right\}w'' + c\dot{w} + \mu\ddot{w} - (Nw')' = 0, \tag{1}$$

$$N = \frac{\mu}{2}\int_s^l ds_1 \int_0^{s_1} (w'^2)''_{tt}\,ds_2,$$

where $\dot{w} = w'_t$, $w' = w'_s$, μ is the mass per unit of length, $c\dot{w}$ is the material damping, and the term $w'''' + \frac{1}{2}(w''w'^2)''$ describes the beam curvature.

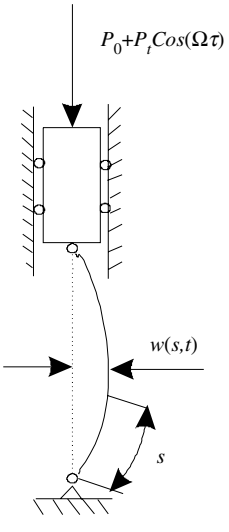

Fig. 1. Transverse beam parametric oscillations are considered. The nonlinear curvature and nonlinear inertia are taken into account

The nonlinear inertia is presented by the term $(Nw')'$ in Eq. (1). The derivation of Eq. (1) is presented in [20]. Let us introduce the dimensionless parameters:

$$\varepsilon\delta = \frac{cl^2}{\sqrt{EJ\mu}},\ \ \varepsilon\delta_L = \frac{c_L w_*^2}{2l\sqrt{EJ\mu}},\ \ \varepsilon\Gamma_t = \frac{l^2 P_t}{EJ},\ \ \Gamma_0 = \frac{P_0 l^2}{EJ},\ \ \varepsilon\gamma = \frac{w_*^2}{2l^2},\ \ m = \frac{M}{\mu l},$$
$$u = \frac{w}{w_*},\ \ \tau = \sqrt{\frac{EJ}{\mu l^4}}t,\ \ \xi = \frac{s}{l},\ \ \Omega = \frac{\bar{\Omega} l^2\sqrt{\mu}}{\sqrt{EJ}},\ \ w_* = \frac{l2\sqrt{2}}{\pi}\sqrt{\frac{P_0}{P_*} - 1}, \tag{2}$$

where $\varepsilon \ll 1$, P_* is the buckling force, and w_* is the static deflection at $s = \frac{l}{2}$. Equation (1) is rewritten in the dimensionless form:

$$u'''' + \Gamma_0 u'' + \ddot{u} + \alpha(u''u'^2)'' + \varepsilon\left[-m\gamma u'' \int_0^1 (u'^2)\ddot{}\, d\xi - \gamma\left(u' \int_\xi^1 d\eta \int_0^\eta (u'^2)\ddot{}\, dh\right)'\right.$$
$$\left. + \delta\dot{u} + \Gamma_t \cos(\Omega\tau)u'' - \delta_L u'' \int_0^1 (u'^2)\dot{}\, d\xi\right] = 0, \tag{3}$$

where $\alpha = w_*^2/(2l^2)$, $u' = u'_\xi$, and $\dot{u} = u'_\tau$.

The dimensionless fundamental frequencies of the linear system (1) have the following values: $p_k = k^2\pi^2$. As follows from the analysis presented in this paper, the frequency Ω is varied in the following range: $0.5 < \Omega < 4$. Therefore, the one mode approximation $u = q(t)\sin(\pi\xi)$ accurately describes the beam dynamics. The following differential equation is derived by the Galerkin method:

$$\ddot{q} + \lambda(q^3 - q) + \varepsilon\left[\gamma\rho\pi^4 q(\dot{q}^2 + q\ddot{q}) + \delta\dot{q} - \Gamma_t\pi^2 q\cos(\Omega\tau) + \delta_L\pi^4\dot{q}q^2\right] + O(\varepsilon^2) = 0, \tag{4}$$

where

$$\lambda = \Gamma_0\pi^2 - \pi^4; \quad \rho = m + \frac{1}{3} - \frac{3}{8\pi^2}. \tag{5}$$

Let us rewrite Eq. (4) in the form:

$$\ddot{q} + \lambda(q^3 - q) + \varepsilon\left[-\gamma\rho\lambda\pi^4(q^5 - q^3) + \gamma\rho\pi^4 q\dot{q}^2 + \delta\dot{q} - \Gamma_t\pi^2 q\cos(\Omega\tau) + \delta_L\pi^4\dot{q}q^2\right] = 0. \tag{6}$$

Note that the system (6) is invariant against the variable change $q \to -q$. We stress that, for $\varepsilon = 0$, (6) is a nonlinear conservative system.

We made calculations with the following parameters [23]:

$$E = 2.013\cdot 10^{11}\frac{N}{m^2},\ \rho = 7.80\cdot 10^3\frac{Kg}{m^3},\ l = 558\,mm,\ b = 11.95\,mm,\ h = 1\,mm,$$
$$M = 0.162\,Kg, \mu = 9.3\cdot 10^{-2}\,\frac{Kg}{m},\ P_* = 6.39N,\ P_0 = 6.42N,\ c = 7.8\cdot 10^{-2}\,\frac{Kg}{s},$$
$$EJ = 0.201\,Nm^2, w_* = 3.4\times 10^{-2}\,m.$$

The dimensionless parameters (2) have the following values:

$$\varepsilon = 0.01,\ \varepsilon\delta = 0.18,\ \Gamma_0 = 10,\ \varepsilon\gamma = 1.84\cdot 10^{-3},\ m = 3.11,\ \rho = 3.4.$$

3 Saddle-node bifurcations

In this section, the Melnikov method [5]–[7] is used to obtain saddle-node bifurcations of limit cycles. It is known that, for $\varepsilon = 0$, the system (6) has periodic solutions of the form:

$$(q_0, \dot{q}_0) = \left\{ \sqrt{\frac{2}{2-k^2}} dn\tau;\ -\frac{k^2\sqrt{2\lambda}}{2-k^2} sn\tau cn\tau \right\}; \quad \tau = t\sqrt{\frac{\lambda}{2-k^2}}, \tag{7}$$

where k is the elliptic integral modulus, and dn, sn and cn are elliptic functions [26], [27]. The equation: $H = \lambda(k^2-1)(2-k^2)^{-2}$ connects the Hamiltonian H of the system (6) for $\varepsilon = 0$ to the modulus of the elliptic integral. Let us consider motions of the system (6) meeting the resonance conditions:

$$T(k) = mT; \quad T = 2\pi/\Omega; \quad T(k) = 2K\sqrt{2 - k^2/\lambda}, \tag{8}$$

where K is the complete elliptic integral of the first kind; $T(k)$ is the period of $\varepsilon = 0$ system orbits. The subharmonic Melnikov method permits to determine the subharmonic oscillations of a single DOF system with essential nonlinear unperturbed part. The simple roots of a subharmonic Melnikov function define these subharmonic oscillations. If subharmonic Melnikov function roots meet the equation $|\sin(\Omega t_0)| = 1$, the saddle-node bifurcation set is derived. The subharmonic Melnikov method is explained in [5].

The subharmonic Melnikov function of the system (6) is derived in the form:

$$\bar{M}_1^{m/1} = -\delta\sqrt{\lambda} J_1(k) + \Gamma_t \pi^2 J_3(k)\sin(\Omega t_0) - \delta_L \pi^4 \sqrt{\lambda} J_2(k), \tag{9}$$

where

$$J_1(k) = \frac{1}{\sqrt{\lambda}} \int_0^{mT} \dot{q}_0^2\, dt = \frac{4}{3}\left[(2-k^2)E - 2k'^2 K\right](2-k^2)^{-3/2},$$

$$J_2(k) = \frac{1}{\sqrt{\lambda}} \int_0^{mT} \dot{q}_0^2 q_0^2\, dt = \frac{8}{15}\left[2(k^4+k'^2)E + (k^2-2)k'^2 K\right](2-k^2)^{-5/2}, \tag{10}$$

$$J_3 \sin(\Omega t_0) = \int_0^{mT} q_0 \dot{q}_0 \cos(\Omega\tau + \Omega t_0) d\tau = \frac{\Omega^2 \pi}{\lambda sh\left(\frac{m\pi K'}{K}\right)} \sin(\Omega t_0).$$

Note that E is the complete elliptic integral of the second kind.

From Eq. (9) we obtain the saddle-node bifurcations set:

$$\Gamma_t = \pm \frac{\sqrt{\lambda}}{\pi^2 J_3(k)}\left[\delta_L \pi^4 J_2(k) + \delta J_1(k)\right]. \tag{11}$$

This bifurcation set on the plane (Ω, Γ_t) are the parameter functions $(\Omega(k), \Gamma_t(k))$:

$$\Omega(k) = \frac{\pi m\sqrt{\lambda}}{K(k)\sqrt{2-k^2}},$$

$$\Gamma_t(k) = \frac{4K^2\sqrt{\lambda}}{3\sqrt{2-k^2}\pi^5 m^2} sh\left(\frac{m\pi K'}{K}\right) \tag{12}$$

$$\times \left[\left(\frac{4\delta_L\pi^4}{5} + \delta\right)(2-k^2)E - \frac{12\delta_L\pi^4 k'^2}{5(2-k^2)}E - 2\left(\frac{\delta_L\pi^4}{5} + \delta\right)k'^2 K\right], \quad 0 \le k \le 1.$$

Using the asymptotic formulae [27], we obtain the following limits:

$$\lim_{k\to 0}\Gamma_t=\begin{cases}0; & m=1,\\ \frac{\sqrt{2\lambda}}{\pi^2}(\delta_L\pi^4+\delta); & m=2,\\ \infty; & m=3,4,\ldots\end{cases}$$
$$\lim_{k\to 1}\Omega=0,\quad \lim_{k\to 1}\Gamma_t=\infty,\quad \lim_{k\to 0}\Omega=m\sqrt{2\lambda}. \tag{13}$$

Figure 2 shows the saddle-node bifurcation curves with the system parameters from Sect. 1. The bifurcation curves of the subharmonic oscillations of orders 1, 2, 3, 4 are denoted by the same numbers (Fig. 2).

The periodic motions of the system (6) for $\varepsilon=0$ outside the homoclinic orbit have the form:

$$(q_0,\dot{q}_0)=\left\{\sqrt{\frac{2k^2}{2k^2-1}}cn\tau;\ -\frac{k\sqrt{2\lambda}}{2k^2-1}sn\tau dn\tau\right\},\quad \tau=\frac{\sqrt{\lambda}t}{\sqrt{2k^2-1}}. \tag{14}$$

In this case, the equation $H=k^2k'^2\lambda(2k^2-1)^{-2}$ connects the Hamiltonian H to the elliptic integral modulus k. The periods of the motion (14) are

$$T(k)=\frac{4K}{\sqrt{\lambda}}\sqrt{2k^2-1}. \tag{15}$$

Let us study periodic motions outside the homoclinic orbit in the system (6). The subharmonic Melnikov functions of these motions are the following:

$$\bar{M}_1^{m/1}=-\delta\sqrt{\lambda}\hat{J}_1(k)+\Gamma_t\pi^2\hat{J}_3(k)\sin(\Omega t_0)-\delta_L\pi^4\sqrt{\lambda}\hat{J}_2(k), \tag{16}$$

where $m=2l;\ l=1,2,\ldots$. The functions $\hat{J}_i(k)$ have the form:

$$\hat{J}_1(k)=\frac{8}{13}\left\{k'^2K-(1-2k^2)E\right\}(2k^2-1)^{-3/2},$$
$$\hat{J}_2(k)=\frac{16}{15}\left\{Kk'^2(k^2-2)+2E(k'^2+k^4)\right\}(2k^2-1)^{-5/2}, \tag{17}$$
$$\hat{J}_3(k)=\frac{2\Omega^2\pi}{\lambda sh\left(\frac{l\pi K'}{K}\right)}.$$

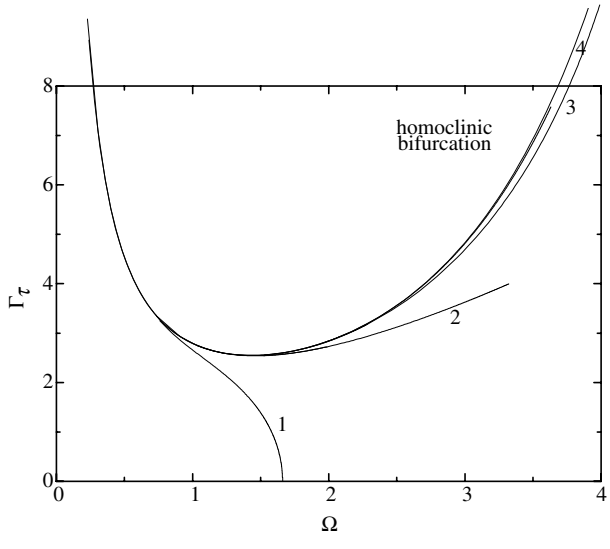

Fig. 2. The saddle-node bifurcation curves of the subharmonic oscillations of orders 1,2,3,4. The curves are denoted by the same numbers. The calculations were produced with the following parameters: $\varepsilon=0.01$, $\varepsilon\delta=\varepsilon\delta_L=0.18$, $\varepsilon\gamma=1.84\cdot 10^{-3}$, $\rho=3.4$

If $J_i(i=\overline{1,3})$ is replaced with $\hat{J}_i$ in formula (9), the saddle-node bifurcation equation of the motions is obtained. These bifurcation sets can be presented by the parameter functions $(\Omega(k), \Gamma(k))$:

$$\pm\Gamma_t(k) = \frac{8\sqrt{\lambda}K^2}{3\ell^2\pi^5(2k^2-1)^{3/2}} sh\left(\frac{\ell\pi K'}{K}\right) \times \left\{Kk'^2\left[\left(\frac{\beta}{5}+\delta\right)k^2 - \frac{4}{5}\beta - \delta\right] + E\left[\frac{2}{5}\beta + \delta + 2\left(\frac{\beta}{5}+\delta\right)(k^2-1)k^2\right]\right\}, \tag{18}$$

$$\Omega(k) = \frac{l\pi\sqrt{\lambda}}{K\sqrt{2k^2-1}}, \quad 1 \le k \le \frac{1}{\sqrt{2}}.$$

The functions (18) have the limits:

$$\lim_{k\to 1}\Omega = 0, \quad \lim_{k\to 1}\Gamma_t = \infty, \quad \lim_{k^2\to\frac{1}{2}}\Omega = \infty, \quad \lim_{k^2\to\frac{1}{2}}\Gamma_t = \infty. \tag{19}$$

Figure 3 shows the saddle-node bifurcation curves (18) of the subharmonic oscillations of orders $m=2$, $m=4$ and $m=6$ for the system parameters from Sect. 1.

Let us consider the saddle-node bifurcations on the plane (δ_L, Γ_t). We study the limit cycles from the right homoclinic orbit. Equation (11) is rewritten in the form:

$$\Gamma_t = \pm\frac{\pi^2\sqrt{\lambda}J_2(k)}{J_3(k)}\left[\delta_L - \delta_L^*(m)\right], \tag{20}$$

where $\delta_L^*(m) = -\frac{\delta J_1(k)}{\pi^4 J_2(k)}$. Following [9], the values $\delta_L^*(m)$ are called the resonance numbers. Figure 4 shows qualitatively the bifurcation curves. Note that the values $\Gamma_t^*(m) = \Gamma_t|_{\delta_L=0}$ have the form:

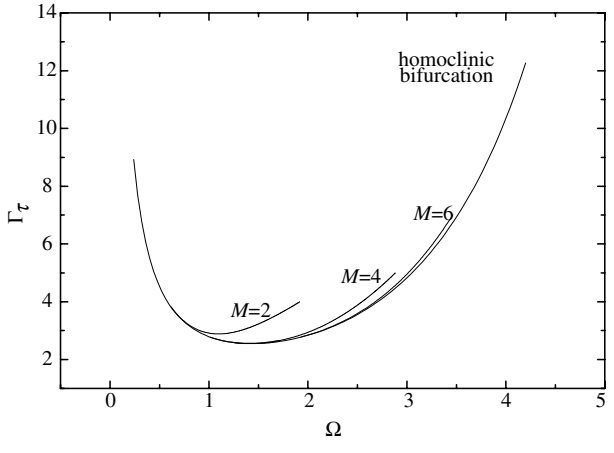

Fig. 3. The saddle-node bifurcation curves of the subharmonic oscillations of orders $m=2$, $m=4$, $m=6$. The parameter function (18) defines these curves. The calculations are produced with the following parameters: $\varepsilon = 0.01$, $\varepsilon\delta = \varepsilon\delta_L = 0.18$, $\varepsilon\gamma = 1.84\cdot 10^{-3}$, $\rho = 3.4$

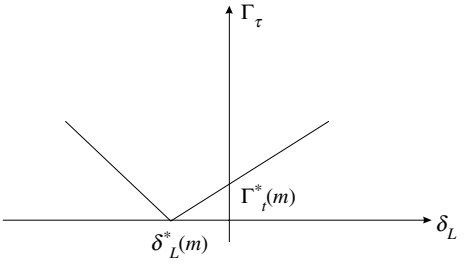

Fig. 4. The qualitative form of the saddle-node bifurcation curve on plane (δ_L, Γ_t). Equation (20) defines these curves

$$\Gamma_t^*(m) = \frac{\delta\sqrt{\lambda}J_1(k)}{\pi^2 J_3(k)}. \tag{21}$$

As the elliptic integral modulus k satisfies the resonance condition (8), the following inequalities are true:

$$k(1) \prec k(2) \prec \cdots \prec k(\infty) = 1. \tag{22}$$

Note that the resonance numbers $\delta_L^*(m)$ satisfy the following relations:

$$\delta_L^*(\infty) = -\frac{5\delta}{4\pi^4}, \quad \lim_{k\to 0}\delta_L^*(m) = -\frac{\delta}{\pi^4}. \tag{23}$$

Using the results of [9], we derive the formula:

$$\begin{aligned}\frac{d}{dk}\delta_L^*(k) = \frac{\delta}{\pi^4 J_2^2 15(2-k^2)}\big[&80(2-k^2)E^2(k) - 160k'^2K(k)E(k) - 32(k^4+k'^2)K(k)E(k)\\ &+16k'^2(2-k^2)K^2(k)\big].\end{aligned} \tag{24}$$

We obtain the following inequality from Eq. (24):

$$\frac{d}{dk}\delta_L^*(k) < 0, \;\; k \in [k_1; 1].$$

Therefore, we can select an integer number m_*, so that

$$-\frac{5\delta}{4\pi^4} = \delta_L^*(\infty) < \cdots < \delta_L^*(m_*+1) < \delta_L^*(m_*). \tag{25}$$

Let us study the intersections of the invariant manifolds of the saddle point. It is known, that these intersections are the necessary condition for the existence of chaos [7]. The homoclinic Melnikov function is derived in the form:

$$M(t_0) = -\frac{4\sqrt{\lambda}\delta}{3} + \frac{\Gamma_t\pi^3\Omega^2}{\lambda sh\left(\frac{\pi\Omega}{2\sqrt{\lambda}}\right)}\sin(\Omega t_0) - \frac{16}{15}\delta_L\pi^4\sqrt{\lambda}. \tag{26}$$

Then invariant manifolds intersections take place if

$$\Gamma_t > \frac{(16\delta_L\pi^4 + 20\delta)\lambda^{3/2}}{15\pi^3\Omega^2} sh\left(\frac{\pi\Omega}{2\sqrt{\lambda}}\right). \tag{27}$$

The homoclinic tangency of manifolds is observed if

$$\Gamma_t = \frac{(16\delta_L\pi^4 + 20\delta)\lambda^{3/2}}{15\pi^3\Omega^2} sh\left(\frac{\pi\Omega}{2\sqrt{\lambda}}\right). \tag{28}$$

Equation (28) meets the following limits:

$$\lim_{\Omega\to+0}\Gamma_t = \infty, \quad \lim_{\Omega\to\infty}\Gamma_t = \infty. \tag{29}$$

Figures 2 and 3 show the manifolds homoclinic tangency curve together with the saddle-node bifurcations curves. Note that on the Fig. 2 scale the manifolds homoclinic tangency curve coincides with the 4th-order subharmonic motions bifurcation curve.

The subharmonic Melnikov function $\bar{M}_1^{m/1}$ and the homoclinic Melnikov function M are connected in the following way:

$$\lim_{m\to\infty}\bar{M}_1^{m/1} = M.$$

4 The bifurcations of motions close to resonance energetic levels

In the previous section, the saddle-node bifurcations were obtained. However, the limit cycles, which undergo these bifurcations, were not studied. It is clear that these cycles may undergo other bifurcations. In this section, we use the Melnikov method, which is considered in the publications [2], [5], [8] to study the other bifurcations of parametric oscillations of beams.

The system (6) with respect to the action-angle coordinates (I, θ) has the form [5]:

$$\dot{I} = \varepsilon F(I, \theta, t); \quad \dot{\theta} = \Omega_\Sigma(I) + \varepsilon G(I, \theta, t), \tag{30}$$

where $\Omega_\Sigma(I)$ is the frequency of the system (6) for $\varepsilon = 0$. Let us consider the following motions:

$$I = I^{m,1} + \sqrt{\varepsilon} h(t); \quad \theta = \Omega_\Sigma(I^{m,1})t + \phi,$$

where the values $I^{m,1}$ are obtained from the resonance conditions (8). Following [8], the system oscillations $I = I^{m,1} + \sqrt{\varepsilon} h(t)$ are called the motions close to the resonance energy level. The aim of the present study is the analysis of the topology of Poincaré sections close to the resonance energy levels. Then the equations of the motion have the following form [5]:

$$\begin{aligned} \dot{\bar{h}} &= \frac{\sqrt{\varepsilon}}{2\pi} \bar{M}_1^{m/1}\left(\frac{\bar{\phi}}{\Omega_\Sigma(I^{m,1})}\right) + \varepsilon \bar{F}_I' \bar{h}, \\ \dot{\bar{\phi}} &= \sqrt{\varepsilon}\frac{\partial \Omega(I^{m,1})}{\partial I}\bar{h} + \varepsilon\left[\frac{\Omega''(I^{m,1})}{2}\bar{h}^2 + \bar{G}(\bar{\phi})\right]. \end{aligned} \tag{31}$$

The functions from Eq. (31) meet the relation:

$$mT\Omega_\Sigma(k)\bar{F}_I' = \bar{M}_1^{m/1}\left(\frac{\bar{\phi}}{\Omega_\Sigma(I^{m,1})}\right). \tag{32}$$

Using the formulae from the Appendix, the system (31) is written in the following form:

$$\begin{aligned} \dot{h} &= \frac{\sqrt{\varepsilon}}{2\pi}\left[-\delta\sqrt{\lambda}J_1(k) + \Gamma_t\pi^2 J_3(k)\sin(m\phi) - \delta_L\pi^4\sqrt{\lambda}J_2(k)\right] \\ &\quad + \varepsilon h\left\{\frac{\Omega(2-k^2)^3}{4\pi m\lambda k^3}\left[-\delta\sqrt{\lambda}J_1' + \Gamma_t\pi^2 J_3'\sin(m\phi) - \delta_L\pi^4\sqrt{\lambda}J_2'\right]\right. \\ &\quad \left. + \frac{\omega(k)}{\Omega}\left(-\delta\sqrt{\lambda}J_1 + \Gamma_t\pi^2 J_3\sin(m\phi) - \delta_L\pi^4\sqrt{\lambda}J_2\right)\right\}, \\ \dot{\phi} &= \sqrt{\varepsilon}\Omega_\Sigma' h + \varepsilon\left\{\frac{\Omega_\Sigma''}{2}h^2 - \frac{\Gamma_t\pi^2\cos(m\phi)}{m}\left[\frac{\Omega(2-k^2)^3}{4\pi m\lambda k^3}J_3' + \frac{\omega(k)}{\Omega}J_3\right] - \gamma\rho\lambda\pi^4\tilde{K}_1(k)\right\}, \end{aligned} \tag{33}$$

where $\omega(k) = -\frac{m}{2\pi}\frac{\partial\Omega_\Sigma}{\partial I}$. The system (33) can be represented in the following way:

$$\begin{aligned} \dot{h} &= \frac{\sqrt{\varepsilon}}{2\pi}\left(-\delta\sqrt{\lambda}J_1 + \Gamma_t\pi^2 J_3\sin m\phi - \delta_L\pi^4\sqrt{\lambda}J_2\right) + \varepsilon h\left(-K_1\delta\sqrt{\lambda} + \Gamma_t\pi^2 K_3\sin m\phi - \delta_L\pi^4\sqrt{\lambda}K_2\right), \\ \dot{\phi} &= \sqrt{\varepsilon}\Omega_\Sigma' h + \varepsilon\left\{\frac{\Omega_\Sigma''}{2}h^2 - \frac{\Gamma_t\pi^2 K_3}{m}\cos m\phi - \gamma\rho\lambda\pi^4\tilde{K}_1(k)\right\}, \end{aligned} \tag{34}$$

where $K_\nu = \frac{\Omega(2-k^2)^3}{4\pi m\lambda k^3}J_\nu' + \frac{\omega(k)}{\Omega}J_\nu$, $\nu = 1, 2, 3$. In this paper, we use the equations of the motion in the form:

$$\dot{h} = \frac{1}{2\pi}\left(-\Delta_1\pi^4\sqrt{\lambda}J_2 + \Gamma_t\pi^2 J_3\sin m\phi\right) + \varepsilon h\left[\chi(\Delta_1) + \Gamma_t\pi^2 K_3\sin m\phi\right];$$

$$\dot{\phi} = \Omega'_\Sigma h + \sqrt{\varepsilon}\left[\frac{\Omega''_\Sigma}{2}h^2 - \frac{\Gamma_t \pi^2 K_3}{m}\cos m\phi\right], \tag{35}$$

where $\Delta_1 = \delta_L - \delta_L^*$; $\quad \chi = \delta\sqrt{\lambda}\frac{\Omega(2-k^2)^2\sigma(k)}{60\pi m\lambda k^3 J_2} - \Delta_1\pi^4\sqrt{\lambda}K_2$,

$\sigma(k) = 80(2-k^2)E^2(k) - 160k'^2K(k)E(k) - 32(k^4+k'^2)K(k)E(k) + 16k'^2(2-k^2)K^2(k)$,

$$K_3 = \frac{\Omega\pi}{\lambda sh\left(\frac{m\pi K'}{K}\right)}\left[\frac{(2-k^2)^3\Omega^2\pi}{8\lambda k^4K^2k'^2}cth\left(\frac{m\pi K'}{K}\right) + \omega(k)\right],$$

$$K_2 = \frac{2E\Omega}{\lambda\pi m\sqrt{2-k^2}} + \frac{\omega(k)}{\Omega}J_2; \quad \Omega'_\Sigma = -\frac{\sqrt{\lambda}\pi^2(2-k^2)[(2-k^2)E - 2k'^2K]}{2K^3k'^2k^4},$$

$$\Omega''_\Sigma = -\frac{\sqrt{\lambda}\pi^3(2-k^2)^{5/2}}{4k^8k'^4}\left[\frac{2E(k'^6+3k'^2+k^4)}{K^4} + \frac{k'^2}{K^3}(4k'^2-k^4) - \frac{3E^2}{K^5}(2-k^2)^2\right].$$

The fixed points of the system (35) are the following ones:

$$(\phi_v, h_v) = \left(\frac{(-1)^v}{m}\arcsin(a) + \frac{\pi v}{m}; 0\right) + O(\varepsilon), \quad v \in Z, \tag{36}$$

where $a = \frac{\sqrt{\lambda}}{\Gamma_t\pi^2 J_3}(\delta J_1 + \delta_L\pi^4 J_2)$. If $a > 0$ $(a < 0)$, then v is changed according to the formula: $v = 0, \ldots, 2m-1$ $(v = 1, \ldots, 2m)$, respectively.

Let us study the stability of these fixed points. The system (35) is linearized and the eigenvalues λ of the constant matrix $[\tilde{A}]$ of the linear system are derived. The values of λ of the saddle fixed points are the following ones:

$$\lambda_{1,2}^{(A)} = \pm\sqrt{\frac{\varepsilon}{2}|\Omega'_\Sigma|\Gamma_t\pi J_3 m\sqrt{1-a^2}} + O(\varepsilon). \tag{37}$$

Other groups of fixed points are denoted by B. The values λ of these fixed points are the following ones:

$$\lambda_{1,2}^{(B)} = \frac{1}{2}tr(\tilde{A}) \pm i\sqrt{\frac{\varepsilon}{2}|\Omega'_\Sigma|\Gamma_t\pi J_3 m\sqrt{1-a^2}}, \tag{38}$$

where $tr(\tilde{A})$ is the trace of matrix $[\tilde{A}]$. Note that the following limit is true:

$$\lim_{k\to 1} tr(\tilde{A}) = \lim_{k\to 1}\varepsilon\frac{\sqrt{\lambda}(\delta_L\pi^4 J_2 + \delta J_1)}{2mTk'^2K(k)}. \tag{39}$$

Motions close to the resonance energy levels have values k near 1. Using formula (39) we conclude that if $\delta_L < \delta_L^*(m)$ $(\delta_L > \delta_L^*(m))$, the fixed points B are stable (unstable), respectively. System (35) is rewritten with respect to $\psi = \phi - a$ (see (36)) to analyze this stability change. Considering the motions close to the fixed point $\psi = 0$ $(|\psi| << 1)$, the following second-order nonlinear equation is derived:

$$\ddot{\psi} + \omega^2\psi = \sqrt{\varepsilon}\dot{\psi}(\alpha + r\psi) + O(\varepsilon), \tag{40}$$

where

$$\alpha = \chi(\Delta_1) + 2\Gamma_t\pi^2 K_3\Delta_1\beta, \ \beta = \frac{\pi^2\sqrt{\lambda}J_2}{\Gamma_t J_3},$$

$$\omega^2 = \frac{|\Omega'_\Sigma|}{2}\Gamma_t\pi J_3 m\sqrt{1-\Delta_1^2\beta^2}, \ r = \frac{\Omega''_\Sigma}{2\Omega'_\Sigma}\Gamma_t\pi J_3 m\sqrt{1-\Delta_1^2\beta^2} + 2\Gamma_t\pi^2 K_3 m\sqrt{1-\Delta_1^2\beta^2}.$$

Let us use the method of averaging [28] to obtain approximate solutions of Eq. (40). Using the change of variables $(\psi, \dot{\psi}) = (a\cos\theta, -a\dot{\theta}\sin\theta)$, the following modulation equations are derived:

$$\dot{a} = \varepsilon \frac{\alpha a}{2} + O(\varepsilon^2); \quad \dot{\theta} = \omega + O(\varepsilon^2), \tag{41}$$

where

$$\alpha(k) = \delta\sqrt{\lambda}\frac{\Omega(2-k^2)^2\sigma(k)}{60\pi m\lambda k^3 J_2} + \Delta_1\pi^4\sqrt{\lambda}\left(2K_3\frac{J_2}{J_3} - K_2\right).$$

As follows from Eq. (41), if $\alpha < 0$ ($\alpha > 0$), the fixed point $\psi = 0$ is asymptotically stable (unstable), respectively. Therefore, the bifurcation set satisfies equation $\alpha = 0$. This equation describes the bifurcation curve H on the parameter plane $(\delta_L, \Gamma_t) \in \mathrm{R}^2$, which can be written in the form:

$$\Delta_1 = \Delta_1^{(H)}(k),$$
$$\lim_{k\to 1}\Delta_1^{(H)}(k) = \frac{15\delta}{8\pi^4\sqrt{\lambda}}\left[\frac{\Omega\pi}{\lambda}cth\left(\frac{\Omega\pi}{2\sqrt{\lambda}}\right) + 1\right]^{-1}\lim_{k\to 1}k'^2K^2. \tag{42}$$

The qualitative location of the bifurcation curve H is shown in Fig. 5. The results of the numerical calculations of this curve are shown in Fig. 6. We stress that as follows from

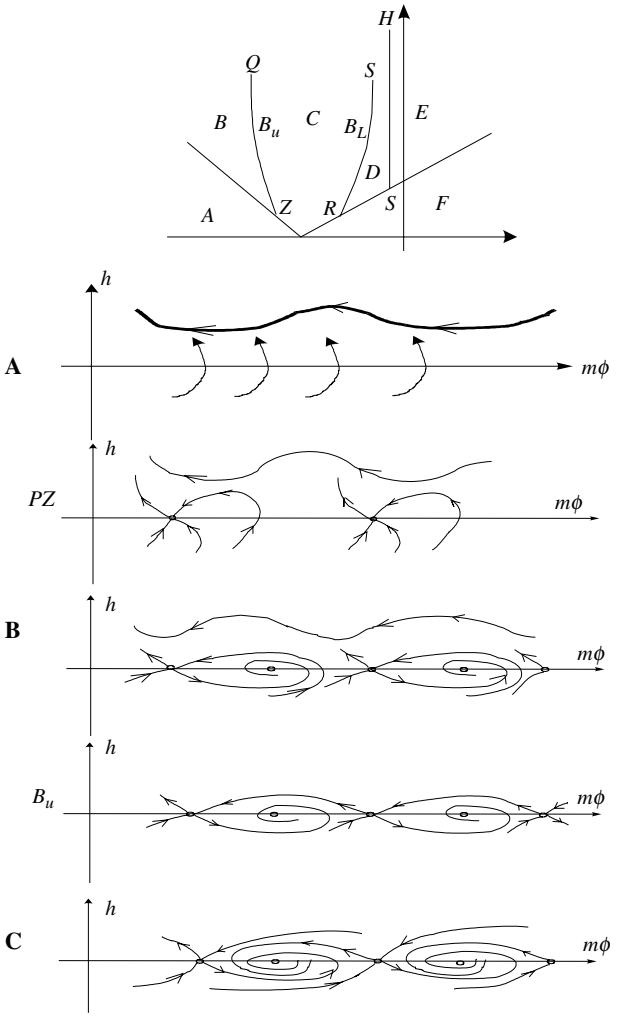

Fig. 5. The curves of the saddle-node bifurcations and the heteroclinic bifurcations (QZ) and (RS) are shown. The letters denote the regions of different dynamical behavior

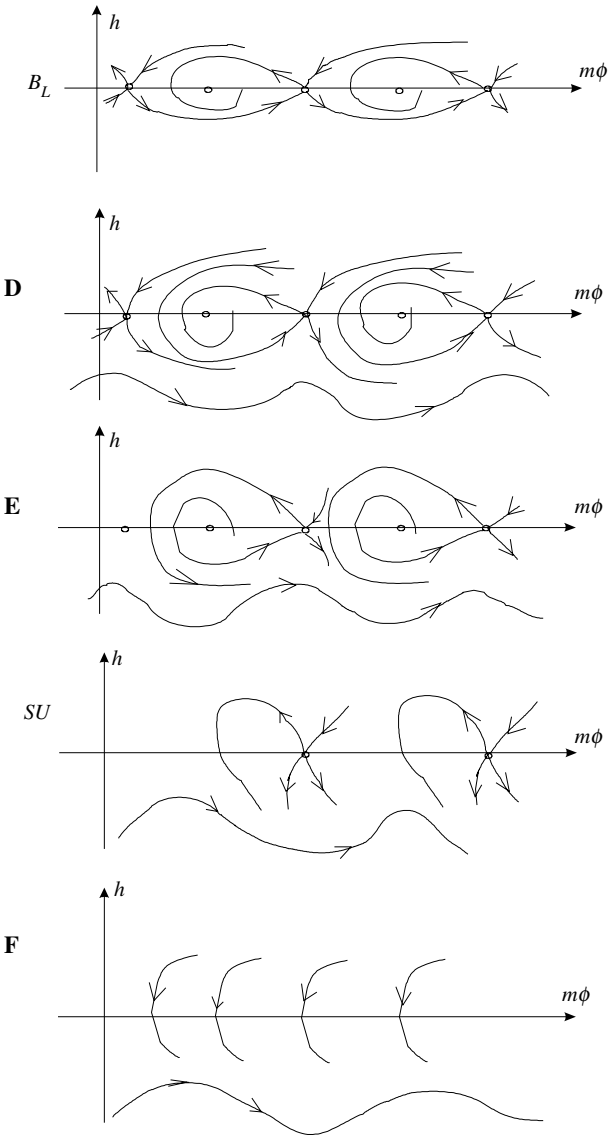

Fig. 5. (Continued)

Eqs. (41), a limit cycle does not arise on the bifurcation curve H. Figure 6 shows the qualitative phase portraits of the system (35) close to the bifurcation curve H.

Let us study homoclinic and heteroclinic orbits of the dynamical system (35). The invariant manifolds of the system (35) for $\varepsilon = 0$ are shown qualitatively on Fig. 7. If $\delta_L \neq \delta_L^*$ and $\delta_L = \delta_L^*$, homoclinic and heteroclinic orbits occur, respectively. The Melnikov function analysis shows, that trajectories topologically equivalent to homoclinic orbits are not observed. Let us consider heteroclinic orbits of the system (35), which are topologically equivalent to the trajectories at $\delta_L = \delta_L^*$ (see Fig. 7). We choose the following values of δ_L:

$$\delta_L = \delta_L^*(m) + \sqrt{\varepsilon}\Delta. \tag{43}$$

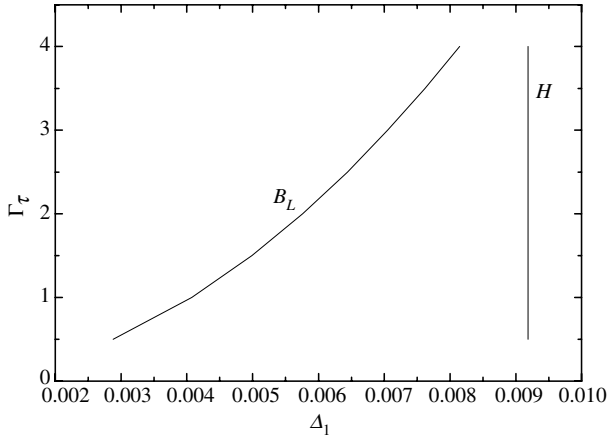

Fig. 6. The bifurcation curves H and B_L, which are presented in Fig. 5, are shown quantitatively for the following parameters: $\varepsilon = 0.01$, $\varepsilon\delta = \varepsilon\delta_L = 0.18$, $\varepsilon\gamma = 1.84 \cdot 10^{-3}$, $\rho = 3.4$

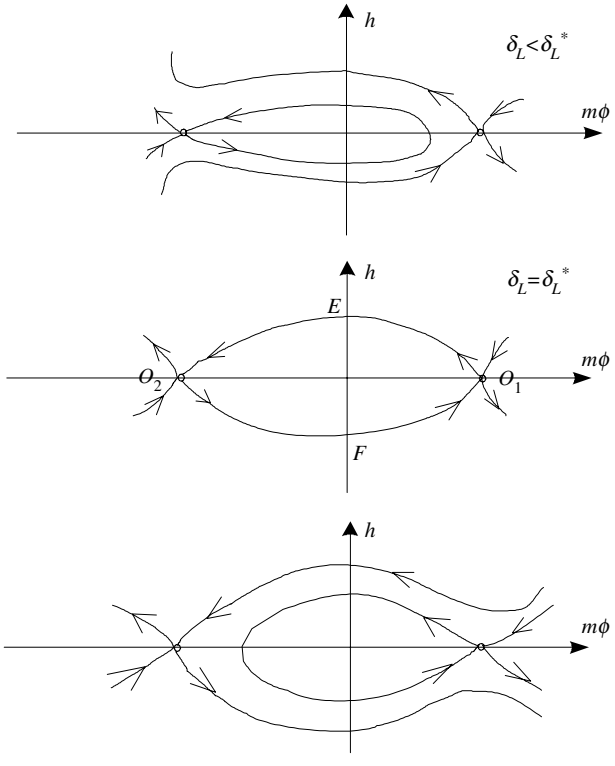

Fig. 7. The qualitative behavior of the homoclinic and heteroclinic orbits of the system (35) for $\varepsilon = 0$ with different parameter δ_L

Then, the system (35) is rewritten in the form:

$$\begin{aligned}
\dot{\phi} &= \sqrt{\varepsilon}\Omega'_\Sigma h + \varepsilon\left(\frac{\Omega''_\Sigma}{2}h^2 - \frac{\Gamma_t \pi^2 K_3}{m}\cos m\phi\right);\\
\dot{h} &= \frac{\sqrt{\varepsilon}\Gamma_t \pi J_3}{2}\sin m\phi + \varepsilon\left\{-\frac{1}{2}\Delta\pi^3\sqrt{\lambda}J_2 + h\left[\chi(0) + \Gamma_t \pi^2 K_3 \sin m\phi\right]\right\}.
\end{aligned} \tag{44}$$

The system (44) without terms $O(\varepsilon)$ has the Hamiltonian K:

$$K = \frac{\sqrt{\varepsilon}\Omega'_\Sigma}{2}h^2 + \frac{\sqrt{\varepsilon}\Gamma_t \pi J_3}{2m}\cos m\phi. \tag{45}$$

This system has saddle fixed points $(\phi_v, h_v) = \left(\frac{2v+1}{m}\pi; 0\right)$; $v = 0; \pm 1; \ldots$ and centers $(\phi_v, h_v) = \left(\frac{2v\pi}{m}; 0\right)$. Note that the heteroclinic orbits join these saddles. Following [5], we derive the Melnikov function to study the heteroclinic bifurcations:

$$M = -\frac{\sqrt{\varepsilon}}{2}\Omega'_\Sigma \Delta\pi^3\sqrt{\lambda}J_2 \int\limits_{-\infty}^{\infty} h\,dt + \sqrt{\varepsilon}\Omega'_\Sigma\chi(0) \int\limits_{-\infty}^{\infty} h^2\,dt. \tag{46}$$

Then the heteroclinic bifurcations set is described by the equations:

$$\Delta = \pm\frac{4\chi(0)}{J_2\sqrt{\lambda}}\sqrt{\frac{2\Gamma_t J_3}{m\pi^7|\Omega'_\Sigma|}}, \tag{47}$$

$$\lim_{k\to 1}\frac{\chi(0)}{J_2\delta\sqrt{\lambda}} = -\frac{15}{32\sqrt{\lambda}}. \tag{48}$$

Equation (47) with minus and plus signs describes the heteroclinic bifurcations of the orbits (O_1 EO_2) and (O_1 FO_2) (see Fig. 7), respectively. These bifurcation sets are denoted by B_u and B_L. Figure 5 shows qualitatively the phase portraits close to the bifurcation curves B_u and B_L.

Let us study the periodic motions of the system (44) meeting the following relations: $\phi(0) = 0; -\phi(t) = \phi(-t)$; $h(t) = h(-t); -\pi < m\phi(t) < \pi$. Using these relations, the subharmonic Melnikov function is derived in the form:

$$\bar{M}_1(K) = \sqrt{\varepsilon}\Omega'_\Sigma \int\limits_{-\tilde{T}/2}^{\tilde{T}/2} \left(-\frac{1}{2}\Delta\pi^3\sqrt{\lambda}J_2 + \chi(0)h\right)h\,dt, \tag{49}$$

where $\tilde{T}$ is the period motion. Function $\bar{M}_1(K)$ has the form:

$$\bar{M}_1(K) = \frac{\Delta\pi^4\sqrt{\lambda}J_2}{m} \mp \frac{4\chi(0)E(k)}{m}\sqrt{\frac{2}{\sqrt{\varepsilon}|\Omega'_\Sigma|}\left(\frac{\sqrt{\varepsilon}\Gamma_t\pi J_3}{2m} - K\right)}, \tag{50}$$

where $k^2 = \frac{\sqrt{\varepsilon}\Gamma_t\pi J_3^2}{\sqrt{\varepsilon}\Gamma_t\pi J_3 - 2Km}$. Formula (50) describes two types of periodic motions.

Equation (50) with the upper (lower) sign determines the motions at $h > 0$ ($h < 0$), respectively. The periodic orbits of the system (44) satisfy the equation $\bar{M}_1(K) = 0$. Therefore, periodic motions meeting the inequalities $h > 0$ and $h < 0$ occur at:

$$\Delta < \frac{4\chi(0)}{\sqrt{\lambda}J_2}\sqrt{\frac{2\Gamma_t J_3}{m|\Omega'_\Sigma|\pi^7}} \quad \text{and} \quad \Delta > -\frac{4\chi(0)}{\sqrt{\lambda}J_2}\sqrt{\frac{2\Gamma_t J_3}{m|\Omega'_\Sigma|\pi^7}}, \tag{51}$$

respectively. If $k \to 1$, the periodic motions are joined to one of the heteroclinic orbits (see Fig. 5).

The dynamical system (35) was studied numerically to confirm the behavior obtained analytically. Changing the parameter δ_L: $\delta_L^{(j)} = \delta_L^{(0)} + jh_L$; $j = \overline{0, 18}$; $\delta_L \in [-0.55; 0.08]$, we calculated the phase plane trajectories of system (35) by the Runge-Kutta method at $\Gamma_t = 2$.

Now let us fix the parameter δ_L to explain the calculations. 100 points were set as the initial conditions in the phase plane domain ($0 < \phi < 2\pi; -40 < h < 40$). We integrated the system (35) from every initial condition. The calculations were finished if the phase plane point was close to a steady state.

The calculations confirmed the system behavior obtained analytically. For example, Fig. 8a shows the periodic motion at $\delta_L = -0.22$. This trajectory corresponds to periodic orbits in region B (see Fig. 5). Figure 8b shows the system's motion to the fixed point at $\delta_L = -0.22$. Figure 8c shows the periodic orbit which corresponds to periodic motions in region D (see Fig. 5).

5 The qualitative behavior of the beam

It is proved in the books [7], [5], that the flow of system (35) is topologically equivalent to the Poincaré sections of system (30). That is, the saddle separatrices of the system (35) are topologically equivalent to the stable and unstable manifolds of the Poincaré map of the system (30). The hyperbolic fixed points of the system (30) correspond to the period m hyperbolic points of the Poincaré sections.

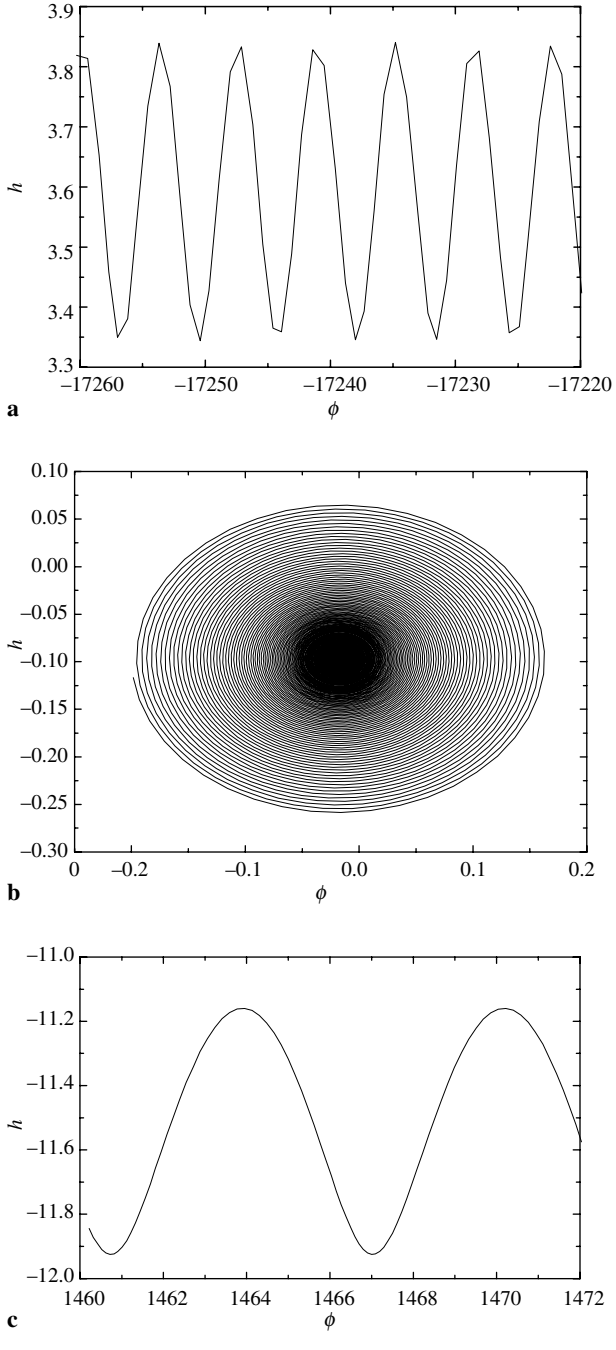

Fig. 8. The system (35) trajectories, which are obtained numerically, are presented; (**a**) shows the periodic motion at $\delta_L = -0.22$; (**b**) demonstrates the system's motion to the fixed point at $\delta_L = -0.22$; (**c**) presents the periodic orbit, which corresponds to periodic motions in region D (see Fig. 5)

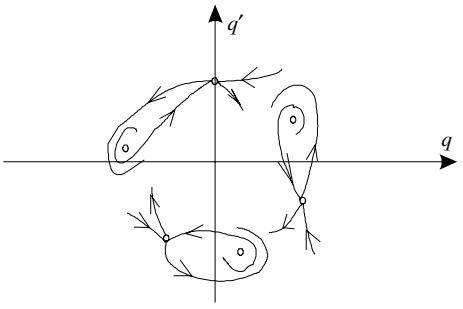

Fig. 9. The qualitative Poincaré sections of the system (35) close to the subharmonic oscillations of order 3. The system parameters correspond to region E (see Fig. 5)

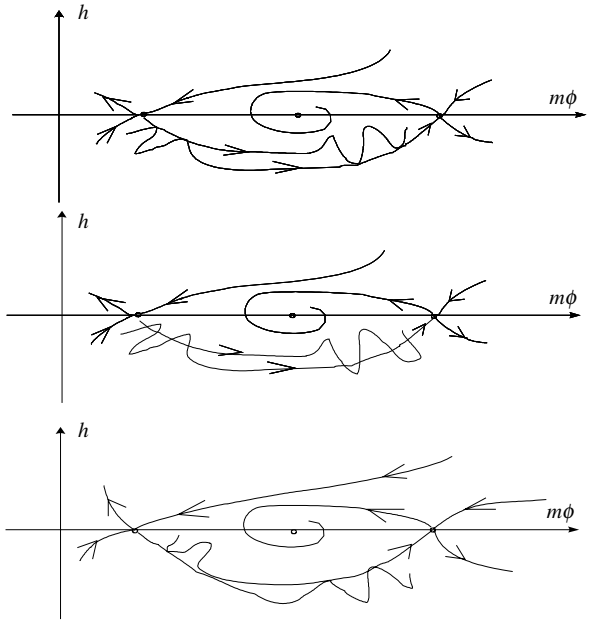

Fig. 10. The qualitative behavior of the invariant manifolds, when the bifurcation curve B_L is intersected

Figure 9 shows qualitatively the Poincaré sections close to the subharmonic oscillations of the order 3. This behavior corresponds to the flow of the system (35) from region E (see Fig. 5).

Let us consider the dynamics of system (6) close to the bifurcation curves B_u and B_L (see Fig. 5). A similar case is considered in [9]. Using results of this paper, we conclude the following. Intersections of the invariant manifolds of the Poincaré sections take place in the vicinity of the bifurcations curves B_U and B_L. These intersections are observed in the small region of the parametric plane (δ_L, Γ_t). The manifolds are touched quadratically at the boundary of this region. Figure 10 shows the qualitative behavior of the invariant manifolds when the bifurcation curve B_L is intersected.

The beam model has $\delta_L > 0$. However, the bifurcation behavior is impossible to study without the analysis of the region $\delta_L < 0$. We stress that the bifurcations behavior has repeated properties. This means that the bifurcations are qualitatively the same for any m. Repeated bifurcations are observed numerically for the frequency modulated CO_2 laser [29].

6 Beam oscillations close to equilibrium

Beam oscillations close to equilibrium $q = 1$ have the form:

$$q(t) = 1 + \sqrt{\varepsilon}x(t). \tag{52}$$

Then, Eq. (6) is written as

$$\ddot{x} + 2\lambda x + \sqrt{\varepsilon}(3\lambda x^2 - \Gamma\cos\Omega t) + \varepsilon(\lambda x^3 - gx + \delta_\Sigma \dot{x} - \Gamma x\cos\Omega t) = 0, \tag{53}$$

where $\Gamma = \Gamma_t\pi^2$; $\delta_\Sigma = \delta + \delta_L\pi^4$; $g = 2\gamma\rho\lambda\pi^4$. Main resonance ($\Omega = \sqrt{2\lambda} + \varepsilon\sigma$; $\Gamma = \bar{\Gamma}\sqrt{\varepsilon}$) of the system (53) is considered in [17]. Therefore, in this paper we consider only the subharmonic resonance.

6.1 Subharmonic resonance $\Omega \approx 2\sqrt{2\lambda}$

The system (53) is analyzed by the multiple scales method [30]. Therefore, we present solutions in the form:

$$x = x_0(T_0, T_1, T_2, \ldots) + \sqrt{\varepsilon}x_1(T_0, T_1, \ldots) + \varepsilon x_2(T_0, \ldots) + \cdots,$$

where $T_0 = t$, $T_1 = \sqrt{\varepsilon}t$ and $T_2 = \varepsilon t$. The following equations are derived:

$$\begin{aligned}
&\frac{\partial^2 x_0}{\partial T_0^2} + 2\lambda x_0 = 0,\ \frac{\partial^2 x_1}{\partial T_0^2} + 2\lambda x_1 = -3\lambda x_0^2 - 2\frac{\partial^2 x_0}{\partial T_0 \partial T_1} + \frac{\Gamma}{2}(\exp(i\Omega T_0) + \exp(-i\Omega T_0)),\\
&\frac{\partial^2 x_2}{\partial T_0^2} + 2\lambda x_2 = -2\frac{\partial^2 x_0}{\partial T_0 \partial T_2} - \frac{\partial^2 x_0}{\partial T_1^2} - 2\frac{\partial^2 x_1}{\partial T_1 \partial T_0} - 6\lambda x_0 x_1 - \lambda x_0^3 + g x_0 - \delta_\Sigma \frac{\partial x_0}{\partial T_0}\\
&\qquad\qquad + \frac{\Gamma x_0}{2}(\exp(i\Omega T_0) + \exp(-i\Omega T_0)).
\end{aligned} \tag{54}$$

Solutions of Eqs. (54) are as follows:

$$\begin{aligned}
x_0 &= A(T_1, T_2)\exp\left(\sqrt{2\lambda}iT_0\right) + \bar{A}(T_1, T_2)\exp\left(-\sqrt{2\lambda}iT_0\right),\\
x_1 &= \frac{\Gamma}{2(2\lambda - \Omega^2)}\exp(i\Omega T_0) + \frac{A^2}{2}\exp(2\sqrt{2\lambda}iT_0) - \frac{3}{2}A\bar{A} + c.c.t,
\end{aligned} \tag{55}$$

where c.c.t. denotes the complex conjugate terms. The modulation equations are determined from the formula:

$$\begin{aligned}
&\frac{\partial^2 x_2}{\partial T_0^2} + 2\lambda x_2 = \exp\left(\sqrt{2\lambda}iT_0\right)\left(-2\frac{\partial A}{\partial T_2}i\sqrt{2\lambda} + 12\lambda A^2\bar{A} + gA - \delta_\Sigma i\sqrt{2\lambda}A\right)\\
&\quad + \Gamma\bar{A}\exp\left(iT_0(\Omega - \sqrt{2\lambda})\right) + un.t.,
\end{aligned} \tag{56}$$

where $un.t.$ denotes summands, which are not source of the secular terms. The subharmonic resonance condition is $\Omega = 2\sqrt{2\lambda} + \varepsilon^2\sigma$. Using the change of variables $A = \frac{a}{2}\exp(i\beta)$, we derive the modulation equations:

$$a' + \frac{\delta_\Sigma}{2}a - \frac{\Gamma a}{2\sqrt{2\lambda}}\sin\psi = 0, \quad \psi' - \sigma_1 - \frac{3\sqrt{\lambda}}{\sqrt{2}}a^2 - \frac{\Gamma}{\sqrt{2\lambda}}\cos\psi = 0, \tag{57}$$

where $\sigma_1 = \sigma + \frac{g}{\sqrt{2\lambda}}$; $\psi = \sigma T_2 - 2\beta$. System (57) has the fixed point $a_0 = 0$ and two other fixed points:

$$a_{1,2}^2 = \frac{\sqrt{2}}{3\sqrt{\lambda}}\left(-\sigma_1 \pm \sqrt{\frac{\Gamma^2}{2\lambda} - \delta_\Sigma^2}\right). \tag{58}$$

Let us use the response surface to analyze the bifurcations of the system. This approach was used by Mira and his coworkers [31] to study the Duffing-Rayleigh system. The response surface shows qualitatively the dependence of fixed points $a_{0,1,2}$ on two parameters σ_1 and Γ (Fig. 11). We stress that the frequency responses are the cross-sections of this surface at $\Gamma = \text{const}$. As one can see from Fig. 11, a response surface represents joining sheets. The sheets of the fixed points $a_{1,2}$ are denoted by the same letters.

The eigenvalues $\lambda_{1,2}$ of the linearized system (57) are derived to study the stability of the fixed points. The values $\lambda_{1,2}$ for the fixed points a_1 are the following:

$$2\lambda_{1,2} = -\delta_\Sigma \pm \sqrt{\delta_\Sigma^2 - 6a_1^2\sqrt{\Gamma^2 - 2\lambda\delta_\Sigma^2}}. \tag{59}$$

The fixed points a_1 are stable. The values $\lambda_{1,2}$ for the fixed points a_2 have the form:

$$2\lambda_{1,2} = -\delta_\Sigma \pm \sqrt{\delta_\Sigma^2 + 6a_2^2\sqrt{\Gamma^2 - 2\lambda\delta_\Sigma^2}}. \tag{60}$$

The fixed points a_2 are unstable. The eigenvalues of the linearized flow close to the fixed point $a_0 = 0$ are the following ones:

$$2\lambda_{1,2} = -\delta_\Sigma \pm \sqrt{-\delta_\Sigma^2 + \frac{\Gamma^2}{\lambda} - 2\sigma_1^2}. \tag{61}$$

The bifurcations of the fixed points a_0 are determined by the equation $\lambda_1 = 0$, which can be written in the form:

$$\frac{\Gamma^2}{2\lambda\delta_\Sigma^2} - \frac{\sigma_1^2}{\delta_\Sigma^2} = 1. \tag{62}$$

Equation (62) presents a hyperbola, which is denoted by pd1 and pd2 (see Fig. 11). The unstable and stable fixed points are arranged above and below this curve, respectively. The saddle-node bifurcation curve sn1 connects the fixed points a_1 to a_2. As follows from Eq. (55), the fixed point a_0 corresponds to the motion of the system (53):

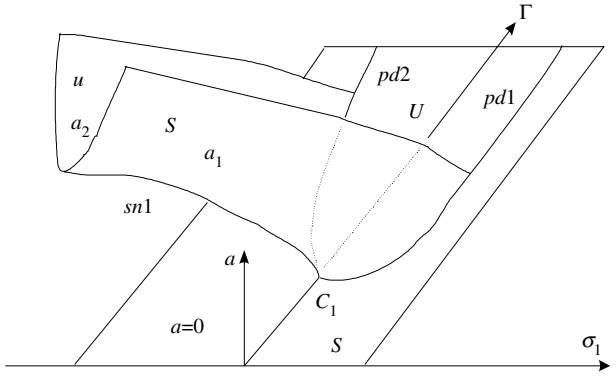

Fig. 11. The response surface of subharmonic resonance $\Omega \approx 2\sqrt{2\lambda}$. The stable and unstable fixed points are denoted by *s* and *u*, respectively. The saddle-node bifurcation of the fixed points is denoted by sn1, and the periodic doubling bifurcations of oscillations of Eq. (6) are denoted by pd1 and pd2

$$x = -\varepsilon \frac{\Gamma}{6\lambda} \cos \Omega t + O(\varepsilon^2). \tag{63}$$

The fixed points $a_{1,2}$ describe the following motions:

$$x = a \cos\left(\frac{\Omega}{2} t - \frac{\psi}{2}\right) + \varepsilon \left[\frac{\Gamma}{6\lambda} \cos \Omega t + \frac{a^2}{4} \cos(\Omega t - \psi) - \frac{3}{4} a^2\right] + O(\varepsilon^2). \tag{64}$$

As follows from Eqs. (63), (64), the period doubling bifurcations take place in the dynamical system (53). Curves pd1, pd2 show these bifurcations (see Fig. 11). Figure 12 shows bifurcation diagrams, which are the sections of the response surface. Let us consider the frequency response, which is shown in Fig. 12a. Note that unstable oscillations are denoted by dotted lines. The frequency response part (AD) describes period $T = \frac{2\pi}{\Omega}$ oscillations. The oscillations (BC) are unstable due to the period doubling bifurcations B and C. Parts (BC) and (CE) describe the unstable and stable oscillations of doubled order, respectively. Figure 12b shows qualitatively the bifurcation diagram (the dependence of the oscillation's amplitudes S on Γ) at $\sigma_1 < 0$. Part (FH) shows the period T oscillations. As the result of period doubling bifurcation G, doubled period unstable oscillations (GI) arise. The doubled period stable oscillations arise due to the saddle-node bifurcation I. Figure 12c shows the bifurcation diagram at $\sigma_1 < 0$. Part (KM) shows the period T oscillations. The period doubling bifurcation takes place at point L. As the result of this bifurcation, stable period 2T oscillations (LP) arise.

6.2 The subharmonic resonance $\Omega \approx 3\sqrt{2\lambda}$

Assuming that $\Gamma = \frac{\bar{\Gamma}}{\sqrt{\varepsilon}}$, subharmonic resonance $\Omega \approx 3\sqrt{2\lambda}$ is considered. Let us present solutions of Eq. (53) in the form:

$$\mathrm{x} = \mathrm{x}_0(\mathrm{T}_0, \mathrm{T}_1, \mathrm{T}_2, \ldots) + \varepsilon^{1/2} \mathrm{x}_1(\mathrm{T}_0, \mathrm{T}_1, \mathrm{T}_2, \ldots) + \varepsilon \mathrm{x}_2(T_0, T_1, T_2, \ldots) + \cdots .$$

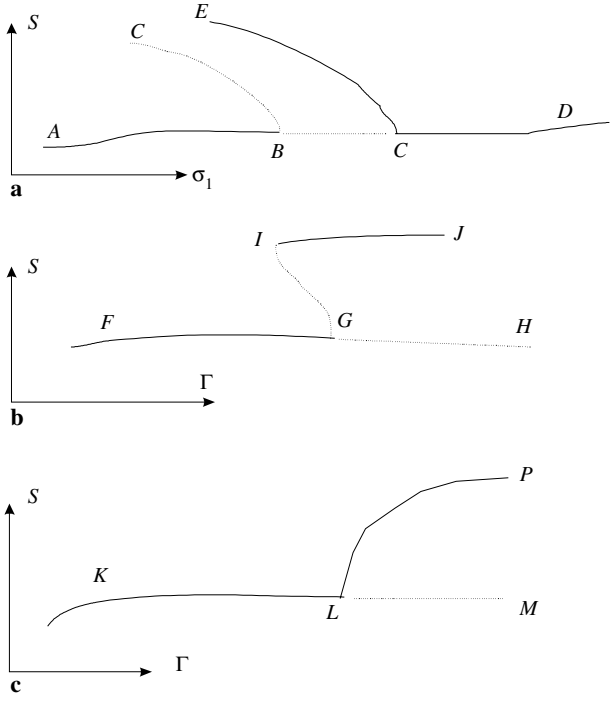

Fig. 12. The bifurcation diagram, which is the section of the response surface (Fig. 11); (**a**) shows the system behavior when σ_1 is varied, and (**b**) and (**c**) show the behavior when Γ is changed. Points B,C,G,L are the period doubling bifurcation points

Using the multiple scales method [30], we derive the equations:

$$\frac{\partial^2 x_0}{\partial T_0^2}+2\lambda x_0=\bar{\Gamma}\cos(\Omega t);\quad \frac{\partial^2 x_1}{\partial T_0^2}+2\lambda x_1=-3\lambda x_0^2+\bar{\Gamma}x_0\cos\Omega t-2\frac{\partial^2 x_0}{\partial T_0\partial T_1}, \tag{65}$$

$$\frac{\partial^2 x_2}{\partial T_0^2}+2\lambda x_2=-2\frac{\partial^2 x_0}{\partial T_0\partial T_2}-\frac{\partial^2 x_0}{\partial T_1^2}-2\frac{\partial^2 x_1}{\partial T_1\partial T_0}-6\lambda x_0x_1+\bar{\Gamma}x_1\cos\Omega t-6\lambda x_0^3+gx_0-\delta_\Sigma\frac{\partial x_0}{\partial T_0}.$$

The subharmonic resonance condition is

$$\Omega=3\sqrt{2\lambda}+\varepsilon^2\sigma_1, \tag{66}$$

where σ_1 is the detuning parameter. Motions of the oscillator (53) are the following:

$$x=A\exp\left(i\sqrt{2\lambda}T_0\right)+\Lambda\exp(i\Omega T_0)+c.c.t.+O(\varepsilon), \tag{67}$$

where $A=\frac{a}{2}\exp(i\beta)$, $\Lambda=\frac{\bar{\Gamma}}{2(2\lambda-\Omega^2)}$; c.c.t. denotes the complex conjugate part of the solutions. Annihilating the secular terms of the third equation of system (65), the following modulation system is derived:

$$\begin{aligned}a'&=-\frac{\delta_\Sigma}{2}a+\frac{a^2\gamma_2}{4\sqrt{2\lambda}}\sin(\sigma_1T_2-3\beta),\\ \beta'&=-\frac{\gamma_3}{2\sqrt{2\lambda}}-\frac{3\sqrt{\lambda}}{2\sqrt{2}}a^2-\frac{a\gamma_2}{4\sqrt{2\lambda}}\cos(\sigma_1T_2-3\beta),\end{aligned} \tag{68}$$

where $\bar{\gamma}_2=\frac{9}{8}\Gamma$; $\gamma_3=g+\frac{7\Gamma^2}{640\lambda}$. We rewrite the system (68) with respect to variables $a,\psi=\sigma_1\mathrm{T}_2-3\beta$:

$$\begin{aligned}a'&=-\frac{\delta_\Sigma}{2}a+\frac{9\Gamma a^2}{32\sqrt{2\lambda}}\sin\psi,\\ \psi'&=\sigma_1^*+\frac{21\Gamma^2}{1280\lambda\sqrt{2\lambda}}+\frac{9\sqrt{\lambda}}{2\sqrt{2}}a^2+\frac{27a\Gamma}{32\sqrt{2\lambda}}\cos\psi,\end{aligned} \tag{69}$$

where $\sigma_1^*=\sigma_1+\frac{3g}{2\sqrt{2\lambda}}$. The dynamical system (69) has the fixed point $a_0=0$ and the other fixed points $a_{1,2}$:

$$a_{1,2}^2=\frac{107\Gamma^2}{7680\lambda^2}-\frac{4\sigma_1^*}{9\sqrt{2\lambda}}\pm\sqrt{\frac{9\Gamma^2}{512\lambda^2}\left(\frac{79\Gamma^2}{7680\lambda^2}-\frac{4\sqrt{2}\sigma_1^*}{9\sqrt{\lambda}}\right)-\frac{2\delta_\Sigma^2}{9\lambda}}. \tag{70}$$

The saddle-node bifurcation curve joins fixed points a_1 to a_2. This bifurcation satisfies the equation:

$$\Gamma^2\left(\frac{237\Gamma^2}{10240\lambda}-\sqrt{2\lambda}\sigma_1^*\right)=\frac{256}{9}\lambda^2\delta_\Sigma^2. \tag{71}$$

By assumption, the magnitude Γ is not too large. Therefore, the value $\frac{237\Gamma^2}{10240\lambda}$ from Eq. (71) can be neglected. Then, the approximate equation of the saddle-node bifurcation is the following:

$$-\sqrt{2\lambda}\sigma_1^*\Gamma^2=\frac{256}{9}\lambda^2\delta_\Sigma^2. \tag{72}$$

Figure 13a shows qualitatively the frequency response of the system (53). The response surface (Fig. 13b) presents the values $a_{1,2}$ in the three-dimensional space $(\sigma_1,\Gamma^2,\mathrm{a})\in\mathrm{R}^3$. This surface represents two sheets connected along the saddle-node bifurcation curve L_1. This curve is a hyperbola (see Fig. 13c).

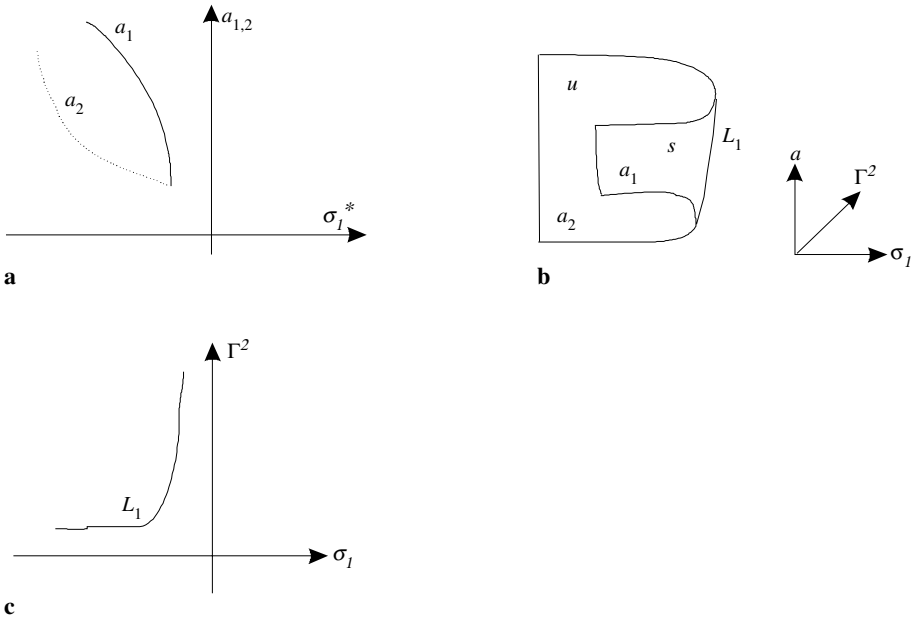

Fig. 13. Bifurcation behavior of the dynamical system; (**a**) the frequency response, (**b**) the response surface, (**c**) the bifurcation curve. The fixed points a_1 and a_2 are stable and unstable, respectively. The curve L_1 is the saddle-node bifurcation curve, which is shown in (**c**)

The eigenvalues $\lambda_{1,2}$ of the linearized flow (69) are derived to study the fixed points stability. These values for the fixed point a_1 are the following:

$$2\lambda_{1,2} = -\delta_\Sigma \pm \sqrt{\delta_\Sigma^2 - 4Ra_1^2}, \tag{73}$$

where

$$R = \frac{9}{2\sqrt{2}}\sqrt{\frac{9\Gamma^2}{256\lambda}\left(\frac{237\Gamma^2}{10240\lambda} - \sqrt{2\lambda}\sigma_1^*\right) - \lambda\delta_\Sigma^2}.$$

The fixed points a_2 have the following values of $\lambda_{1,2}$:

$$2\lambda_{1,2} = -\delta_\Sigma \pm \sqrt{\delta_\Sigma^2 + 4a_2^2R}. \tag{74}$$

Therefore, the fixed point a_1 is asymptotically stable and the fixed point a_2 is a saddle, which is shown on the response surface (see Fig. 13).

Note that the fixed points correspond to the following motions of the system (53):

$$x = a\cos\left(\frac{\Omega}{3}t - \frac{\psi}{3}\right) + 2\Lambda\cos\Omega t + O(\varepsilon). \tag{75}$$

7 Numerical simulations of beam oscillations

The objective of these calculations is the bifurcation analysis of the system (6) for a variation of the parameter Γ_t and keeping the parameter Ω constant at $\Omega = 2\sqrt{2\lambda}$. We integrate the system

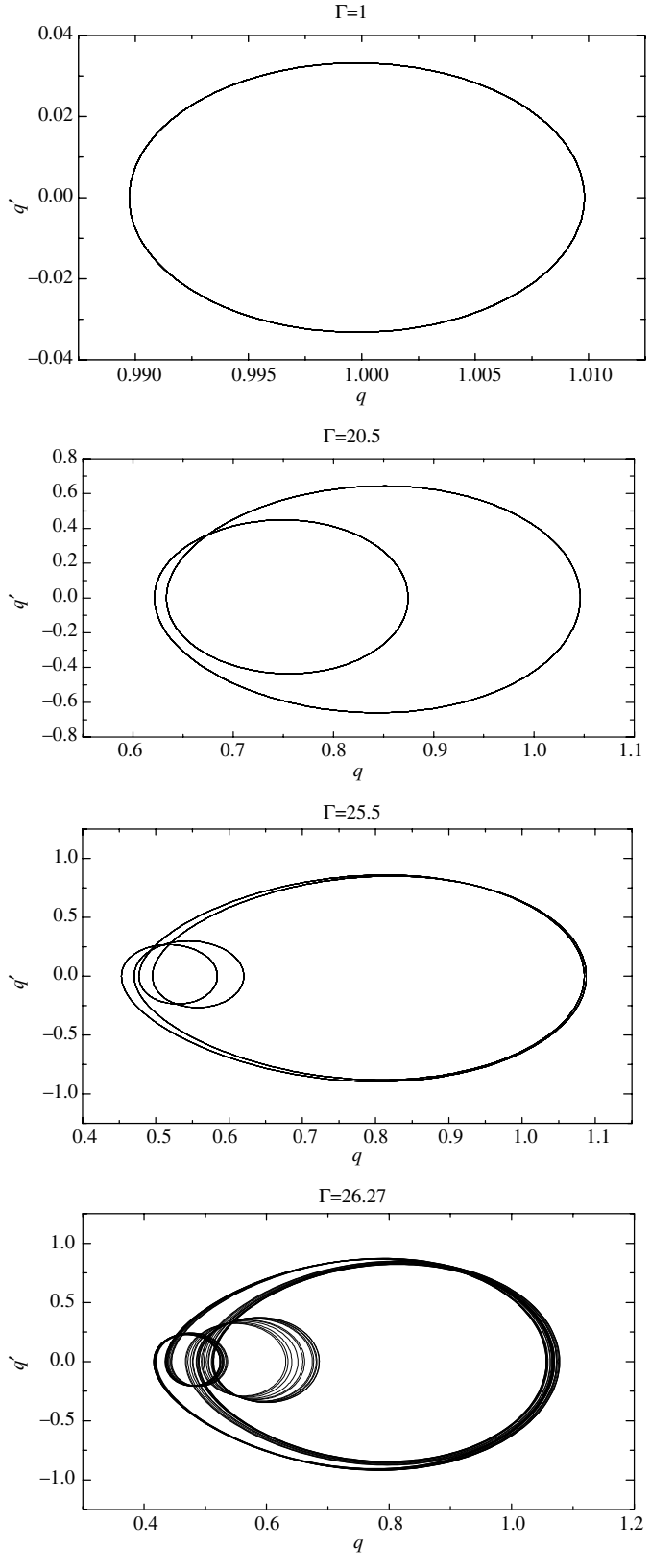

Fig. 14. The system (6) motions obtained by numerical integration

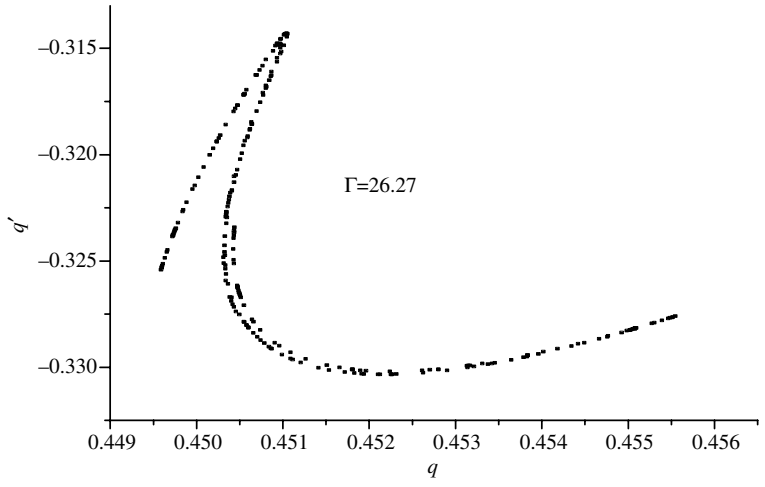

Fig. 15. The Poincaré sections of the chaotic attractor

(6) by the Runge-Kutta method. The numerical values of the system (6) parameters are presented in the second section.

Let us consider the approach for the calculations with constant Γ_t. The rectangle

$$D = \left\{(q, \dot{q}) \in R^2 / 0 < q < 3.14; -0.6 < \dot{q} < 0.6\right\}$$

was filled by 450 points. Every point was used as initial condition to integrate the system (6). After defining all steady states, the value Γ_t was changed, and all calculations were carried out once more.

As result of the calculations, the following system behavior was obtained. The motions with the excitation period take place at $\Gamma_t \in [1; 19.5]$. For example, Fig. 14 shows the limit cycle at $\Gamma_t = 1$ in the plane $(q, \dot{q}) \in R^2$. The doubled order cycle is observed at $\Gamma_t = 20.5$. This cycle is shown on Fig. 14, too. We conclude that a period doubling bifurcation takes place. Such cycles exist at $\Gamma_t \in [20.5; 24.5]$. The motions of the four times the excitation period take place at $\Gamma_t = 25.5$ (see Fig. 14). Such oscillations occur at the region $\Gamma_t \in [25.5; 26.0]$. A chaotic attractor appears at $\Gamma_t = 26.27$. Figure 15 shows the Poincaré sections of this attractor.

The period doubling bifurcations considered in this section are studied analytically in Sect. 6.1. As follows from the analytical analysis, the first period doubling bifurcation takes place at $\Gamma_t = 17$. Numerical simulation shows that this bifurcation takes place at $\Gamma_t \approx 19.9$.

Numerical simulations show that besides the considered above steady states, trajectories, which escape to infinity, occur.

8 Conclusions

Nonlinear parametric oscillations of beams with regard to the nonlinear inertia and nonlinear curvature are considered in this paper. The beam has three equilibria as the compressive force is larger than the statical buckling force. The single-mode approximation is used to present the beam motions. The second-order differential equation is derived by Galerkin's method. Melnikov's method is used to study this equation. The bifurcations of the parametric oscillations of the beam are analyzed by Melnikov's method. It is shown in this paper, that the bifurcation behavior is repeated qualitatively for any order of the subharmonic motions.

The bifurcations of the nonlinear oscillations of the beam close to equilibrium are studied by the multiple scales method. The analytical results are compared with numerical simulation data.

Appendix

$$\bar{G} = \bar{G_1} + \bar{G_2};$$

$$\bar{G_1} = -\frac{1}{mT}\int_0^{mT} \frac{\partial q_0}{\partial I}\left[\gamma\rho\lambda\pi^4(q_0^5 - q_0^3) - \gamma\rho\pi^4 q_0\dot{q}_0^2 - \delta\dot{q}_0 - \delta_L\pi^4\dot{q}_0 q_0^2\right]dt = -\gamma\rho\lambda\pi^4 K_1(k);$$

$$mT\tilde{K_1}(k) = \frac{\partial}{\partial I}\int_0^{mT}\left(\frac{q_0^6}{4} - \frac{q_0^4}{2}\right)dt - h_0(k)\frac{\partial}{\partial I}\int_0^{mT} q_0^2 dt;$$

$$h_0(k) = \frac{k^2 - 1}{(2 - k^2)^2};$$

$$\bar{G_2} = -\frac{\Gamma_t\pi^2}{mT}\int_0^{mT}\frac{\partial q_0}{\partial I} q_0\cos(\Omega\tau + m\phi)d\tau = -\frac{\Gamma_t\pi^2}{m^2T}\frac{\partial}{\partial I}\left(\frac{J_3}{\Omega_\Sigma}\right)\cos(m\phi);$$

$$\bar{G_2} = \int \frac{\partial\bar{F_2}}{\partial I}\, d\phi;$$

$$\frac{\partial\bar{F_2}}{\partial I} = \frac{\partial}{\partial I}\frac{\Gamma_t\pi^2}{\Omega_\Sigma mT}\int_0^{mT} q_0\dot{q}_0\cos(\Omega\tau + m\phi)d\tau.$$

Acknowledgment

The author especially thanks Profs. Yu. V. Mikhlin, O. Morachkovski, J. Awrejcewicz, and A.G. Petrov for many useful conversations on the topics presented in this article and the reviewer for suggestions, which significantly improve the paper.

References

[1] Vol'mir, A.S.: Nonlinear dynamics of plates and shells. Moscow: Nauka 1972 (in Russian).
[2] Melnikov, V.K.: On the stability of the center for time periodic perturbations. Trans. Moscow Math. Soc. **12**, 1–56 (1963).
[3] Holmes, P.: A nonlinear oscillator with a strange attractor. Phil. Trans. Royal Soc. London **292**, 419–448 (1979).
[4] Holmes, P., Whitley, D.: On the attracting set for Duffing's equation. I: Analytical methods for small force and damping. In: Partial differential equations and dynamical systems (Fitzgibbon, W.E. ed.), pp. 121–154. London: Pitman 1984.

[5] Guckenheimer, J., Holmes, P.: Nonlinear oscillations, dynamical systems and bifurcations of vector fields. New York: Springer 1983.
[6] Morozov, A.D.: Global analysis in theory of nonlinear oscillations. Niznij Novgorod: Novgorod University 1995 (in Russian).
[7] Wiggins, S.: Introduction to applied nonlinear dynamical systems and chaos. New York: Springer 1990.
[8] Morozov, A.D.: Approach to a complete qualitative study of Duffing's equation. USSR J. Comp. Math. Math. Phys. **13**, 1134–1152 (1973).
[9] Greenspan, B., Holmes, P.: Repeated resonance and homoclinic bifurcation in a periodically forced family of oscillators. SIAM J. Math. Anal. **15**, 69–97 (1984).
[10] Morozov, A.D.: A complete qualitative investigation of Duffing's equation. Differential Equations **12**, 164–174 (1976).
[11] Morozov, A.D., Shilnikov, L.P.: On nonconservative periodic systems close to two-dimensional Hamiltonian. Prikl. Mat. Mekh. **47**, 327–334 (1984).
[12] Morozov, A.D., Shilnikov, L.P.: On mathematical theory of oscillations synchronization. DAN SSSR **223**, 1340–1343 (1975) (in Russian).
[13] Morozov, A.D.: On resonance and chaos in parametric systems. Prikl. Mat. Mekh. **58**, 41–51 (1994).
[14] Moon, F.C.: Experiments on chaotic motions of a forced nonlinear oscillator: strange attractor. Trans. ASME. J. Appl. Mech. **47**, 638–644 (1980).
[15] Chason, R., Bejarano, J.D.: Homoclinic and heteroclinic chaos in a triple-well oscillator. J Sound Vibr. **186**, 269–278 (1995).
[16] Holmes, C., Holmes, P.: Second-order averaging and bifurcations to subharmonic in Duffing's equation. J. Sound Vibr. **78**, 161–174 (1981).
[17] Yagasaki, K.: Second-order averaging and Melnikov analysis for forced nonlinear oscillators. J. Sound Vibr. **190**, 587–609 (1996).
[18] Lenci, S., Tarantino, A.M.: Influence of the excitation shape in the classical Duffing equation. Eur. J. Mech. **13**, 569–579 (1994).
[19] Lenci, S., Menditto, G., Tarantino, A.M.: The chaotic resonance. Eur. J. Mech A/Solids **13**, 857–866 (1994).
[20] Bolotin, V.V.: The dynamic stability of elastic systems. San Francisco: Holden-Day 1964.
[21] Evensen, H.A., Ivan-Iwanowski, R.M.: Effect of longitudinal inertia upon the parametric response of elastic column. ASME J. Appl. Mech. **33**, 144–148 (1966).
[22] Eisinger, K., Merchaut, H.C.: Clamped beam parametric amplifier. ASME J. Appl. Mech. **46**, 197–202 (1979).
[23] Saito, H., Koizumi, N.: Parametric vibrations of a horizontal beam with a concentrated mass at one end. Int. J. Mech. Sci. **24**, 755–761 (1982).
[24] Sato, K., Saito, H., Otomi, K.: The parametric response of a horizontal beam carrying a concentrated mass under gravity. ASME J. Appl. Mech. **45**, 643–648 (1978).
[25] Fung, R.F.: The effect of nonlinear inertia on the steady-state response of a beam system subjected to combinated excitations. J. Sound Vibr. **203**, 373–387 (1997).
[26] Ahiezer, N.I.: Elements of elliptic functions theory. Moscow: Nauka 1948 (in Russian).
[27] Abramowitz, M., Stegun, I.A.: Handbook of mathematical functions. Dover: Gorden and Breach 1965.
[28] Bogolubov, N.N., Mitropolski, Yu. A.: Asymptotic methods in the theory of nonlinear oscillations. New York: Gorden and Breach 1961.
[29] Mira, C., Djellit, I.: Bifurcation structure in a model of a frequency modulated CO_2-laser. I. J. Bifurcation Chaos **3**, 97–111 (1993).
[30] Nayfeh, A.H.: Perturbation methods. New York: Wiley 1973.
[31] Qriouet, M., Mira, C.: Fractional harmonic synchronization in the Duffing-Rayleigh differential equation. I.J. Bifurcation Chaos **4**, 411–426 (1994).

Author's address: Dr. K. V. Avramov, Department of Theoretical Mechanics, National Technical University "Kharkov Polytechnical Institute", Frunze St. 21, Kharkov 61002, Ukraine (E-mail: kvavr@kharkov.ua)